ACS Catalysis

Research Article

pubs.acs.org/acscatalysis

Substantial Pretreatment Effect on CO Oxidation over Controllably Synthesized Au/FeO_x Hollow Nanostructures via Hybrid Au/β-FeOOH@SiO_2

Bo Sun,[†] Xinzhen Feng,[†] Yao Yao,[†] Qin Su,[†] Weijie Ji,*[,†] and Chak-Tong Au*[,‡]

[†]Key Laboratory of Mesoscopic Chemistry, School of Chemistry and Chemical Engineering, Nanjing University, Nanjing 210093, China

[‡]Department of Chemistry, Hong Kong Baptist University, Kowloon Tong, Hong Kong

ABSTRACT: A novel synthetic strategy has been adopted to deposit Au nanoparticles (NPs) (ca. 5 nm) on a hollow FeO_x substrate using Au/β-FeOOH hybrid nanocrystals as the precursor. Through the encapsulation of Au/β-FeOOH by SiO_2 shells and the calcination step, the Au/β-FeOOH can be transformed into Au/FeO_x with the hollow structural feature. Because of the protective SiO_2 shells, aggregation of the Au NPs is effectively prohibited, and the hemispherical morphology of the Au particles is essentially retained. The Au/FeO_x hollow composite is obtained by removing the SiO_2 shells, and the Au NPs in the final Au/FeO_x hollow composite are small-sized yet stable enough because of the calcination history. The derived Au/FeO_x hollow composite shows a substantial pretreatment effect on CO oxidation: with a pretreatment in the reaction feed at 180 °C for 0.5 h, the hollow Au/FeO_x shows the T_{100} of CO oxidation decreasing from 180 to 88 °C. O_2 temperature-programmed desorption and X-ray photoelectron spectroscopy characterizations revealed that the pretreatment may result in (i) the creation of electron holes in the p-type FeO_x substrate and electron deficiency of Au nanoparticles as well as a strong Au−FeO_x interaction; (ii) appropriate coverage of oxygen adspecies on the Au NPs; and (iii) increased surface oxygen density, especially at the Au−FeO_x boundary region, as a result of the spillover effect of oxygen adspecies from Au NPs. All of these features are responsible for an overall enhanced activity of CO oxidation and better durability of the Au/FeO_x hollow composite.

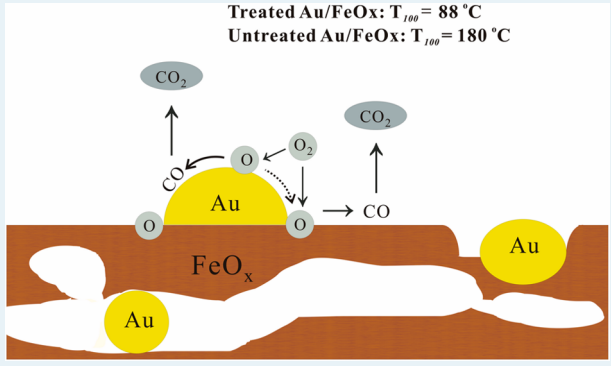

KEYWORDS: *gold, akagenite, hematite, hollow nanostructures, pretreatment effect, CO oxidation*

1. INTRODUCTION

Composite nanostructures[1−3] comprising two or more chemically different constitutions have attracted increasing interest from materials scientists because of their novel properties and unique applicability that cannot be achieved with single constitution. The properties of a composite nanomaterial can be dramatically changed by varying its composition as well as assembled structure. Therefore, many efforts have been made to fabricate various nanocomposite materials to accomplish serendipitous multifunctionality.

Since the discovery in the late 1980s that gold (Au) is catalytically active when it is dispersed as small particles on oxide supports, the preparation of Au-based catalysts has been widely studied.[2,4−13] The catalytic activity was found to depend strongly on the dimension of the Au particles, the support material, the synthetic method, and the activation procedure. However, in spite of their good initial catalytic activity, supported Au catalysts have few commercial applications. Deactivation of the Au nanoparticle (NP)-based catalysts is complicated from one system to another. One of the key issues is the stability of the Au nanocatalysts under reaction conditions. When the interaction between Au and the support is weak, the Au particles migrate on the surface of support through Ostwald ripening, producing larger Au particles and losing their catalytic activity for CO oxidation. The activity of supported Au NPs depends on the type and structure of the support.[14−19] The mobility of supported Au NPs is rather high, resulting in their tendency to aggregate at various temperatures.[20−24] The reported highly active supported Au NPs are seldom subject to calcination, and their activity can hardly be maintained for long periods.[25−28] Therefore, the concerns to stabilize the supported Au NPs have continued. Zenella et al.[29] loaded Au particles on yttrium-modified TiO_2, and the catalysts showed higher activity as well as better stability than Au/TiO_2 in CO oxidation. Yan et al.[30] used binary mixed oxides as Au supports. They first coated TiO_2 with a thin layer of Al_2O_3 via a surface sol−gel method and then loaded Au NPs. Zhu et al.[31] reported a rational design of Au/TiO_2-based catalysts with

Received: July 1, 2013
Revised: November 13, 2013
Published: November 14, 2013

   dx.doi.org/10.1021/cs4009732 | ACS Catal. 2013, 3, 3099−3105

enhanced thermal stability through postmodification of Au/TiO_2 by amorphous SiO_2 decoration. Jin recently reviewed the synthesis of different metal NPs with precious control in size, composition, and morphology and their potentials in catalysis.[32] The current study aimed to enhance the durability of Au NPs by reducing the aggregation tendency of the Au NPs through a unique synthetic strategy. The Au NPs were dispersed on the iron oxide substrate with encapsulation by SiO_2 shells and then subjected to air calcination at 600 °C. Because of the protective SiO_2 shells, aggregation of the Au NPs was effectively prohibited (from 3.7 ± 0.8 nm in Au/β-FeOOH to 4.6 ± 1.5 nm in hollow Au/FeO_x), and meanwhile, the hollow structural feature of the iron oxide substrate was created by the calcination treatment. After removal of the SiO_2 shells, the Au NPs in the final Au/FeO_x hollow composite are small-sized yet stable enough (showing stable activity up to 60 h) because of the calcination history and resulting strong Au−substrate interaction.

Over the past decade, hollow nanostructures with enhanced pore volume and controlled shell thickness have emerged as an important class of functional materials.[33,34] These hollow nanostructures show higher surface to volume ratios compared with solid counterparts of the same size, making them attractive for the fields of catalysis, energy storage and conversion, and biomedicine. There are plenty of successful examples of the construction of different kinds of hollow structures in recent years.[35−38] The fabrication of Co_3O_4 nanotubes by means of a modified Kirkendall effect has been recently reported by us, and the derived materials showed excellent activity and good stability toward the catalytic combustion of CH_4.[39] However, these hollow structures generally contain a single ingredient, and less attention has been directed toward the fabrication of hollow nanostructures of multiple components.

Fe_2O_3 is a versatile component for a wide range of applications such as catalysis,[40] gas sensing[41] and lithium batteries.[42] In this context, we devoted our attention to the development of a Au/FeO_x composite with the novelty of a hollow structural feature. A schematic illustration of the nanostructure design employed in this study is shown in Scheme 1.

Scheme 1. Illustration of the Strategy for Synthesizing the Hollow Au/FeO_x@SiO_2 and Au/FeO_x Hybrid Nanostructures

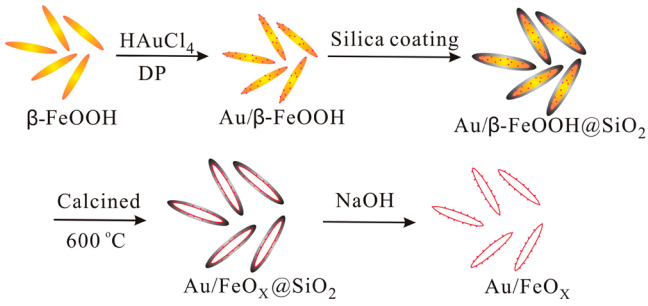

2. EXPERIMENTAL SECTION

2.1. Catalyst Preparation. *Preparation of β-FeOOH.* $FeCl_3$ (1.48 g) and poly(vinylpyrrolidone) (PVP) (2.28 g) were dissolved in distilled water, and the resulting solution was sealed in a Teflon-lined autoclave and kept at 373 K for 10 h. After that, the materials were collected by centrifugation, washed with distilled water three times, and dried at room temperature (RT) overnight.

Preparation of Au/β-FeOOH. A deposition−precipitation method was employed for Au introduction. The pH of an $HAuCl_4 \cdot 3H_2O$ solution (0.01 M) was adjusted to 8.0 using a KOH solution (1.0 M), and the resulting solution was heated to 80 °C. Then the as-synthesized β-FeOOH was added, and the slurry was magnetically stirred for 3 h. The nominal Au loading was 3% by weight. The solids were centrifuged and washed three times with distilled water, dried at 80 °C overnight, and calcined in a muffle oven at 250 °C for 3 h.

Preparation of Au/β-FeOOH@SiO_2. In a typical synthesis, Au/β-FeOOH was dispersed in a mixture containing 15 mL of ethanol and 7.5 mL of ammonium hydroxide, and the suspension was sonicated for 30 min in an ultrasound cleaner (KQ-100DE, 40 kHz, 100 W). Subsequently, a certain amount of TEOS was injected into the suspension under sonication. After 90 min, the products were collected by centrifugation, washed with distilled water, and dried at 80 °C overnight.

Preparation of Au/FeO_x@SiO_2. The Au/β-FeOOH@SiO_2 composite was heated to 600 °C in air and kept at this temperature for 5 h.

Preparation of the Au/FeO_x Hollow Composite. The Au/FeO_x@SiO_2 nanostructures were immersed in a NaOH solution (0.4 M) under sonication for 3 h to remove the silica shells. The solids were isolated by centrifugation, washed with water, and dried at RT. The Au content in the final sample was 1.7 wt % as determined by the ICP-AES technique.

Preparation of Au/Bulk FeO_x. A solution of $Fe(NO_3)_3 \cdot 9H_2O$ (1 mol L^{-1}, 10 mL) was added dropwise (5 mL min^{-1}) to a solution of Na_2CO_3 (1 mol L^{-1}, 100 mL) at RT under vigorous stirring. After 1 h, the precipitate was isolated and washed thoroughly with warm water until the pH of the supernatant reached 7. Au loading was performed as in the synthesis of Au/FeOOH, and the derived sample was then calcined in a muffle oven at 600 °C for 5 h.

2.2. Catalyst Activity Test. The catalytic activity of CO oxidation was evaluated in a continuous-flow fixed-bed reactor operated at atmospheric pressure. The catalyst (50 mg) was placed in a quartz tube reactor. The as-synthesized Au/β-FeOOH and Au/β-FeOOH@SiO_2 were used directly without further treatment, while the Au/Fe_2O_3 hollow composite was pretreated in a flow of reaction feed at 180 °C for 30 min. The feed gas (1.6% CO, 21.0% O_2, balance N_2) was passed through the catalyst bed at a total flow rate of 25 mL min^{-1}, giving a corresponding gas hourly space velocity (GHSV) of 30 000 cm^{-3} g^{-1} h^{-1}. The inlet and outlet gas compositions were analyzed online using a gas chromatograph (GC-122).

2.3. Characterization of Catalysts. X-ray diffraction (XRD) analysis was conducted on a Philips X'Pert MPD Pro X-ray diffractometer with Cu Kα radiation (λ = 0.1541 nm) in the 2θ range of 10−80°. Transmission electron microscopy (TEM) images were taken on a JEOL JEM-1010/2010 transmission electron microscope operated at 200 kV. X-ray photoelectron spectroscopy (XPS) analysis was performed on a PHI 5000 Versaprobe system using monochromatic Al Kα radiation (1486.6 eV) operating at 25 W. The sample was outgassed overnight at RT in an ultrahigh-vacuum chamber (<5 × 10^{-7} Pa). All binding energies (BEs) were referenced to the C 1s peak at 284.6 eV. Temperature-programmed desorption of oxygen (O_2-TPD) was carried out using a U-shaped quartz reactor. The catalyst (100 mg) was pretreated in an Ar stream at 120 °C for 1 h, and oxygen adsorption proceeded with

dx.doi.org/10.1021/cs4009732 | ACS Catal. 2013, 3, 3099−3105

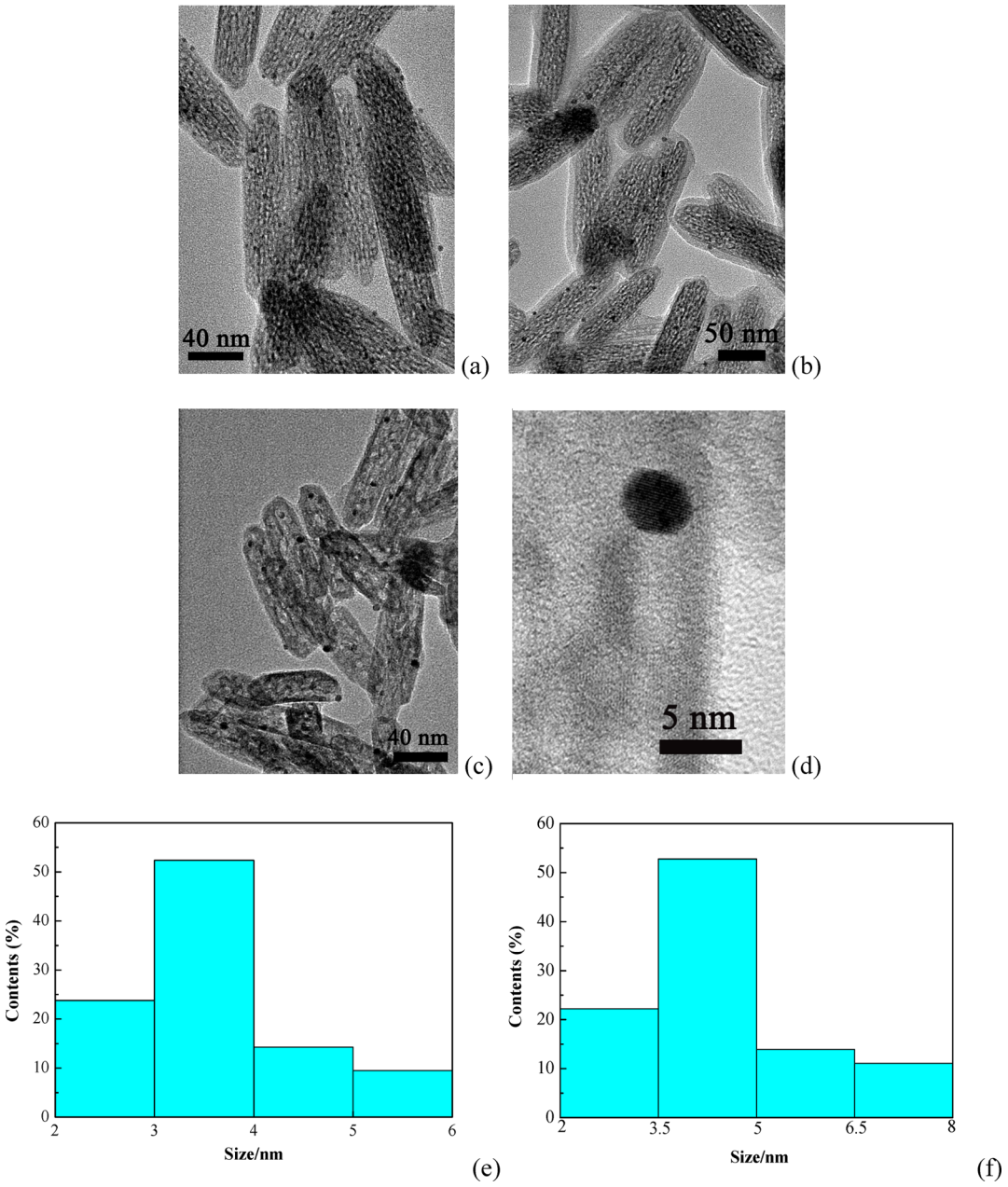

Figure 1. (a–c) TEM images of (a) Au/β-FeOOH, (b) Au/β-FeOOH@SiO_2, and (c) Au/FeO_x. (d) HRTEM image of a Au NP in Au/FeO_x. (e, f) Au particle size distributions in (e) Au/β-FeOOH and (f) Au/FeO_x.

exposure to pure O_2 at RT for 0.5 h. The sample was purged in an Ar flow (60 mL min^{-1}) for 1 h and then heated to 600 °C at a rate of 10 °C min^{-1} in an Ar flow (60 mL min^{-1}), and the effluent gas was analyzed using a thermal conductivity detector.

3. RESULTS AND DISCUSSION

3.1. TEM/XRD. The monodispersed spindle-shaped akagenite (β-FeOOH) NPs with diameters of ca. 20 nm and lengths of 150–180 nm were first synthesized through the hydrolysis of a diluted aqueous iron chloride solution in the presence of PVP. With a controlled deposition–precipitation method, Au NPs were found to be distributed on the β-FeOOH NPs (Figure 1a). Core–shell-structured Au/β-FeOOH@SiO_2 NPs were obtained by coating a thin silica layer on the Au/β-FeOOH NPs. The TEM image indicates that the Au/β-FeOOH NPs were encapsulated by thin silica shells with a thickness of ca. 10 nm (Figure 1b). The silica coated Au/β-FeOOH NPs were then subjected to thermal treatment in air at 600 °C for 5 h. Upon this calcination, the inner akagenite species shrank remarkably, and a hollow structure was developed (Figure 1c). The creation of the hollow structure is due to the volume reduction resulting from the phase transformation of structurally looser β-FeOOH to denser hematite and the strong interface association between the silica shell and the FeO_x specimen.[33] The protective SiO_2 shells were readily removed by aqueous NaOH solution. It can be observed from Figure 1c,d that the Au NPs were distributed on the walls and cavities of the FeO_x hollow structure and essentially retained their particle size (from 3.7 ± 0.8 to 4.6 ± 1.5 nm; Figure 1e,f). It is commonly recognized that Au NPs easily suffer from a significant activity drop upon high-temperature calcination.[43] This situation may adversely influence the application of Au

dx.doi.org/10.1021/cs4009732 | ACS Catal. 2013, 3, 3099–3105

NPs when the operation and regeneration of catalysts at elevated temperature are needed.[44] Decorating the dispersed Au NPs with a thin layer of amorphous SiO_2 is a potential straightforward solution to improve the stability of the Au NPs and hence the catalytic performance. In this study, the SiO_2 shells not only isolated the Au/β-FeOOH nanostructures to prevent them from aggregation upon calcination but also provided an essential base to generate the Au/FeO_x hollow composite while maintaining high dispersion of the Au NPs. Therefore, the novel Au/FeO_x hollow nanostructure with high specific surface area can be obtained. After the thermal treatment and elimination of the SiO_2 shells, the Au NPs basically retained the originally hemispherical morphology (Figure 1d). In addition, the powder XRD patterns (Figure 2) confirmed the β-FeOOH phase structure (JCPDS card no. 34-1266).

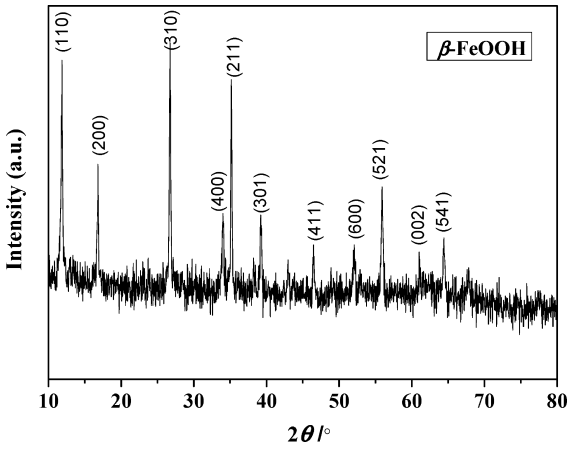

Figure 2. XRD pattern of the β-FeOOH NPs.

3.2. Catalytic Activity. In the fields of exhaust emission control and fuel cells, Au NPs deposited on metal oxide supports are among the most prevalent systems to explore the catalytic oxidation of CO to CO_2.[45,46] Hence, the novel Au/FeO_x hollow nanostructures were investigated in CO oxidation as a model reaction. Various samples with identical Au/Fe atomic ratios were compared, namely, treated and untreated Au/β-FeOOH, untreated Au/β-FeOOH@SiO_2, the treated Au/FeO_x hollow composite, Au/bulk FeO_x, and the commercial Au catalyst reference sample.[47] The pretreatment was performed at 180 °C for 0.5 h in the reaction feed [CO/O_2/N_2 = 1.6/21/77.4 (v/v/v)]. Figure 3 shows the plot of CO conversion versus reaction temperature over different nanostructures. According to the values of T_{100} (the temperature at which 100% CO conversion is achieved), the catalysts showed the following sequence for CO oxidation activity: treated hollow Au/FeO_x (T_{100} = 88 °C) > untreated Au/β-FeOOH (T_{100} = 150 °C) > untreated hollow Au/FeO_x (T_{100} = 180 °C) > treated Au/β-FeOOH ≈ Au/bulk FeO_x (T_{100} = 255 °C) > untreated Au/β-FeOOH@SiO_2 (T_{100} = 300 °C) (Figure 3). The pretreated hollow Au/FeO_x showed significantly enhanced catalytic activity upon pretreatment. The commercial Au catalyst showed a low-temperature activity between those of untreated and treated Au/β-FeOOH, while its T_{100} value was the highest among all of the samples compared. According to Figure 4, at a conversion level of 85%, the untreated Au/β-FeOOH was significantly deactivated, especially in the first 30 h, whereas the treated hollow Au/FeO_x maintained its activity

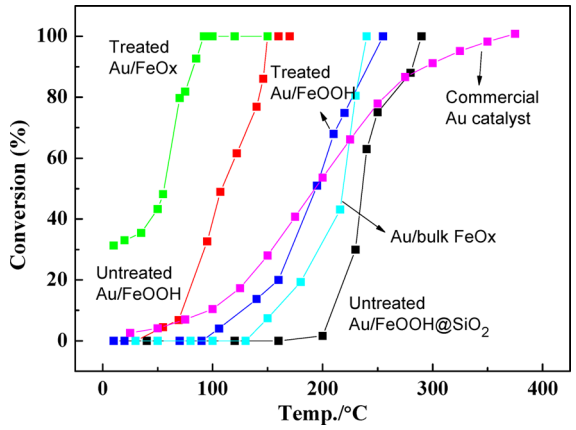

Figure 3. Temperature dependence of CO conversion over various Au-containing nanostructures (the activity of a commercial Au catalyst under similar reaction conditions was adopted from ref 47).

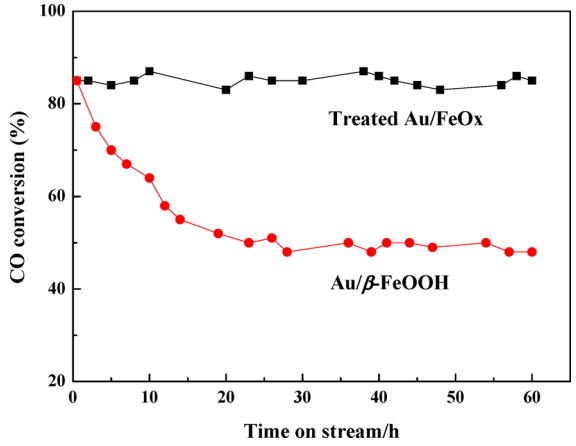

Figure 4. Stabilities of Au/β-FeOOH and treated hollow Au/FeO_x as functions of time on stream (the initial CO conversion for both catalysts was controlled to be approximately 85%).

well within a period of 60 h. It is thought that the good catalyst durability of the pretreated hollow Au/FeO_x may originate from the calcination history of Au/β-FeOOH@SiO_2 at 600 °C. Similar observations were made over Au/Y_2O_3–TiO_2,[29] Au/TiO_2,[31] and Pt/CeO_2.[48] Usually the precalcination treatment would enhance the catalyst durability at the expense of Au particle growth, giving lower catalytic activity. Haruta and coworkers[49] found that the CO oxidation activity of Au NPs drops with increasing calcination temperature. In the current study, because of the presence of the SiO_2 shell and intensive Au–SiO_2 interaction, the growth of Au NPs was effectively suppressed (a size increase from 3.7 ± 0.8 nm in Au/β-FeOOH to only 4.6 ± 1.5 nm in hollow Au/FeO_x), even though the Au/β-FeOOH@SiO_2 was subjected to high-temperature calcination. Furthermore, the texture of hollow FeO_x substrate is beneficial for dispersion of the Au NPs and also physically suppresses the tendency of Au NPs to aggregate because they are located in different cavities of the hollow FeO_x substrate. On the other hand, because of the strong interaction between the SiO_2 shell and Au/FeO_x, the SiO_2 shell may cause some of the Au sites to be inaccessible and also result in a diffusion limitation issue, which leads to an activity drop (see the results for the untreated Au/FeO_x@SiO_2 in Figure 3). This result

dx.doi.org/10.1021/cs4009732 | ACS Catal. 2013, 3, 3099–3105

implies that it is beneficial to remove the SiO_2 shells for better catalytic activity (Scheme 1).

It is interesting to find out that the pretreatment history in the reaction atmosphere can have a remarkable impact on the activity of Au/FeO_x hollow nanostructures in CO oxidation: for instance, the pretreated hollow Au/FeO_x showed only T_{100} = 88 °C while the hollow Au/FeO_x without pretreatment showed T_{100} = 180 °C. Nie et al.[50] recently reported that oxygen pretreatment of $Au_{25}(SR)_{18}$ nanoclusters supported on CeO_2, TiO_2, and Fe_2O_3 oxides at 150 °C resulted in a notable enhancement in the CO oxidation activity [particularly for the $Au_{25}(SR)_{18}/CeO_2$ system], implying that CO oxidation can be directly catalyzed by the intact $Au_{25}(SR)_{18}/CeO_2$. In contrast, Gaur et al.[51] found that the air-dried $Au_{38}(SC_{12}H_{25})_{24}$ clusters supported on TiO_2 are nearly inactive for CO oxidation. The pretreatment presumably leads to a redox cycle of $M^{n+} \rightleftarrows M^{m+}$, as suggested for Au/$CeO_2$ by Widmann et al.[52] and for Au/FeO_x by Li et al.[53] It is worth noting that the activity of Au/β-FeOOH (pretreated or not) was lower than that of treated hollow Au/FeO_x (Figure 3), suggesting although the presence of Au NPs enhances oxygen activation, as previously observed over Au/Mn_3O_4 by us,[54] the nature of the substrate (FeO_x vs β-FeOOH in the current study) also plays an important role in CO oxidation even if the morphology and size of the Au NPs are essentially unchanged. There are several possible parallel reaction pathways for CO oxidation over the catalyst surface: one is over the Au NPs, another is over the hollow FeO_x substrate, while the third is at the Au–FeO_x interfaces. According to the previous studies,[54−57] the oxide substrate can involve the oxidation of CO or hydrocarbon reactant. The degree of such oxidation, however, is dependent upon the type of oxide substrate and also the metal–substrate combination. In the present case, it is certain that the contribution of the iron oxide substrate to CO oxidation is insignificant compared with that of the Au–FeO_x boundary region. Our earlier study[54] on Au/regularly-shaped Mn_3O_4 NPs suggests that the activated oxygen species over the Au NPs can spillover onto the region of the Au–FeO_x interfaces, where they further react with the adsorbed CO to generate CO_2. Clearly, this supplementary pathway may also contribute to the overall activity of CO oxidation in the current study (Scheme 2). A recent study of the Au–Ni/SiO_2 model catalysts illustrates the critical role of the NiO-on-Au interface in CO oxidation.[58] Moreover, Au–Co/SiO_2 and Au–Fe/SiO_2 were also found to promote the Au-catalyzed CO oxidation reaction, confirming the importance of the transition-metal oxide (TMO)-on-Au architecture for CO oxidation.

Scheme 2. Possible Reaction Pathways for CO Oxidation over the Au/FeO_x Nanocatalyst

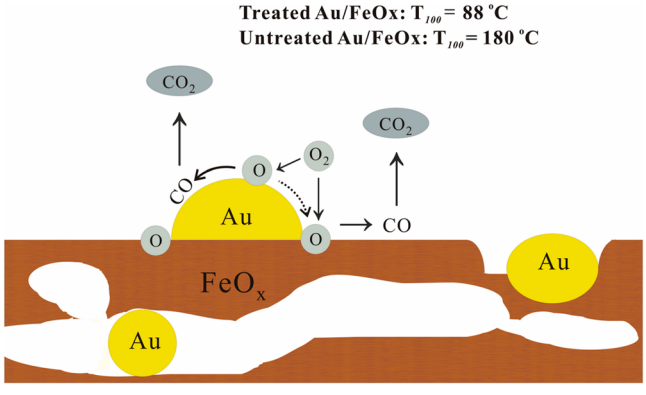

3.3. O_2-TPD. In order to better understand the effect of the pretreatment on the nature of the Au/FeO_x hollow nanostructure, O_2-TPD and XPS techniques were employed to study the treated and untreated samples. The O_2-TPD profiles are shown in Figure 5. According to the results

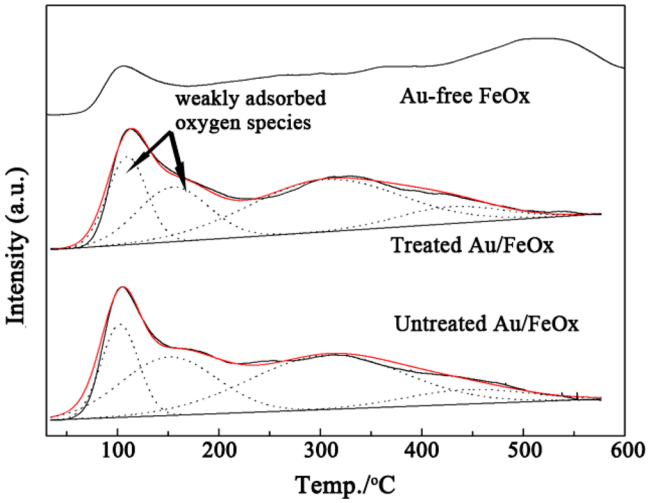

Figure 5. O_2-TPD profiles of the treated and untreated hollow Au/FeO_x nanostructures and Au-free FeO_x.

reported by Xue et al.,[59] the desorption peak below 300 °C can be ascribed to the desorption of weakly adsorbed oxygen species such as O^{2-} and O^-, while the one above 350 °C can be attributed to the desorption of lattice oxygen species. Generally, the desorption peaks in the 100–300 °C range correspond to the oxygen species that are more active for catalytic oxidation. In terms of the area of desorption peak(s) associated with the oxygen adspecies, it is clear that the Au NPs introduced into the FeO_x substrate promote oxygen adsorption, similar to the observation made on the Au/Mn_3O_4 system.[54] On the basis of the curve-fitting analysis, it is observed that the intensities of the desorption peaks of oxygen adspecies decrease after the pretreatment, implying a decline in adsorbed oxygen density on the treated Au/FeO_x. As a matter of fact, FeO_x is a typical p-type semiconductor; the pretreatment of Au/FeO_x in the reaction atmosphere at 180 °C could result in the generation of cation vacancies accompanied by the creation of electron holes to maintain charge balance, as well as interstitial metal atoms in the substrate crystal. This would favor charge transfer from the Au NPs to the FeO_x substrate, leading to the positively charged Au NPs as evidenced by the XPS results (see section 3.4). The positively charged Au NPs also bring about relatively low density of oxygen adspecies (Figure 5), which is coincident with the observation made by Widmann et al.[52] that a slightly lower density of oxygen adspecies on the Au NPs corresponds to a higher CO oxidation activity.

3.4. XPS. The results of the XPS investigation of the pretreated and untreated samples are shown in Figure 6. For the untreated Au/FeO_x, the BEs of Au $4f_{7/2}$ and Au $4f_{5/2}$ were 83.5 and 87.3 eV, respectively, while for the pretreated one, the BEs were 84.0 and 87.7 eV, respectively (Figure 6a). Although the Au NPs were essentially in the metallic state according to the corresponding BE values,[6] increments of Au BEs in the pretreated Au/FeO_x imply electron deficiency of Au NPs upon

dx.doi.org/10.1021/cs4009732 | ACS Catal. 2013, 3, 3099–3105

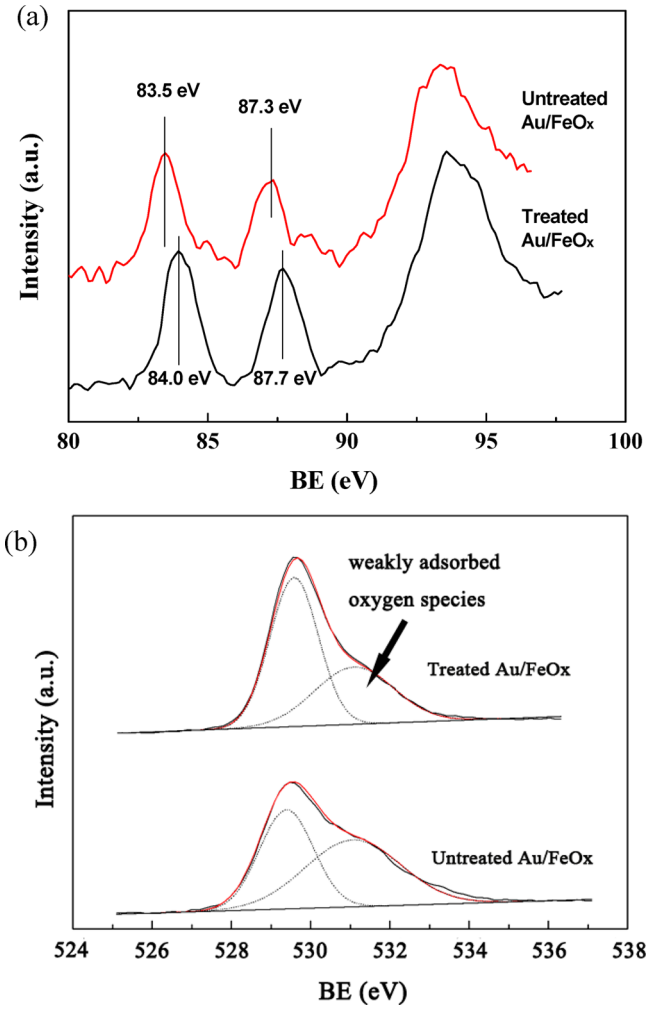

Figure 6. (a) Au 4f and (b) O 1s XPS spectra of the treated and untreated hollow Au/FeO_x nanostructures.

in situ pretreatment.[60] The results for the O 1s signals of treated and untreated Au/FeO_x obtained by curve-fitting analysis (Figure 6b), together with those of O_2-TPD (Figure 5), clearly reveal that after the pretreatment, there was a smaller amount of oxygen adspecies on the Au NPs,[61,62] coincident with the Au 4f XPS signals of positively charged Au NPs in the pretreated Au/FeO_x. This is understandable since cation vacancies (or excess oxygen anions) could be generated in the p-type FeO_x substrate upon the pretreatment in the current study. As a result, electron holes would be simultaneously created, favoring electron transfer from Au NPs to substrate, especially at the Au−FeO_x boundary. This would lead to electron deficiency of Au NPs in the pretreated Au/FeO_x[63] and a comparatively low density of oxygen adspecies on the Au NPs. When the catalyst surface is partly hydroxylated, the CO oxidation could occur via the formation of surface formate species. Since the electron-deficient Au NPs are favorable for the generation of surface formate species, they can enhance the CO oxidation activity.[64] The surface Au concentrations measured by XPS were essentially identical before and after pretreatment, suggesting that the change in Au dispersion was insignificant, as revealed earlier by the TEM observations (Figure 1a,c). With the protection of the SiO_2 shells, the aggregation of Au NPs was effectively minimized during the high-temperature calcination. After removal of the protective SiO_2 shells, the stabilized Au NPs can scarcely aggregate under the milder conditions for CO oxidation.

Applying the technique of temporal analysis of products (TAP), Widmann et al.[52] demonstrated that calcined Au/CeO_2 was only slightly active for CO oxidation and that the small amount of surface oxygen should be removed before the catalyst reaches its more active steady-state surface composition. The activity was notably increased on a catalyst surface with lower surface oxygen concentration (by a reduction of approximately 7%), while the over-reduction of surface oxygen coverage may cause lower initial activity. Interestingly, the current study shows that the Au NPs subjected to a pretreatment in the reaction feed behaved exactly as electron-deficient species, as evidenced by the XPS results (Figure 6), giving rise to a relatively low surface oxygen concentration on the Au/FeO_x (Figures 5 and 6). Without pretreatment, the Au/FeO_x hollow composite showed T_{100} = 180 °C for CO oxidation, while the activity increased substantially (T_{100} = 88 °C) upon pretreatment at 180 °C. Moreover, the spillover of oxygen adspecies from Au NPs onto the Au−FeO_x boundary region could not only reduce surface oxygen coverage on the Au NPs but also add extra oxygen anions around the Au−FeO_x boundary, where the coming oxygen species could react with the neighboring adsorbed CO to give CO_2 as an additional route for CO oxidation on Au/FeO_x.

4. CONCLUSIONS

Deposition of Au NPs (4−5 nm) on the hollow FeO_x substrate [30−50 nm (Φ) × 150−180 nm (*L*)] was achieved using Au/*β*-FeOOH hybrid nanocrystals as precursors. By coating of a SiO_2 layer on the Au/*β*-FeOOH and a calcination step (600 °C for 5 h), Au/FeO_x with a hollow structural feature was obtained. Because of the protection of the SiO_2 shells, the Au NPs retained high dispersion even when Au/FeO_x was subjected to high-temperature calcination. The Au/FeO_x hollow nanostructure free of the SiO_2 shell was obtained by treatment with NaOH solution. The Au NPs in the final Au/FeO_x composite were small-sized yet stable enough for CO oxidation. The synthesized Au/FeO_x hollow composite exhibited a significant pretreatment effect on the CO oxidation activity: the T_{100} of Au/FeO_x was notably decreased from 180 to 88 °C. The characterizations by O_2-TPD and XPS suggested that the applied pretreatment brings about the generation of electron holes in the p-type FeO_x substrate, which leads to electron deficiency of the Au NPs. Electron-deficient Au NPs result in a slightly lower coverage of oxygen adspecies on the Au NPs. Increased surface oxygen density is expected especially at the Au−FeO_x boundary as a result of the spillover effect of oxygen adspecies from the Au NPs. All of these aspects are thought to be responsible for the overall enhanced activity in CO oxidation.

AUTHOR INFORMATION

Corresponding Authors

*Tel: +86-25-83686270. Fax: +86-25-83317761. E-mail: jiwjnju@yahoo.com; jiwj@nju.edu.cn.
*Tel: +852-34117810. E-mail: pctau@hkbu.edu.hk.

Notes

The authors declare no competing financial interest.

■ ACKNOWLEDGMENTS

Financial support from the MSTC (2013AA031703), NSFC (21173118), NSFJS (BK2011439), and MOE (20110091110023) is greatly appreciated.

■ REFERENCES

(1) Wang, X.; Liu, D. P.; Song, S. Y.; Zhang, H. J. *Chem. Commun.* **2012**, *48*, 10207−10209.
(2) Li, G. J.; Lu, F. F.; Wei, X.; Song, X. P.; Sun, Z. B.; Yang, Z. M.; Yang, S. C. *J. Mater. Chem. A* **2013**, *1*, 4974−4981.
(3) Yeo, K. M.; Shin, J.; Lee, I. S. *Chem. Commun.* **2010**, *46*, 64−66.
(4) Haruta, M.; Kobayashi, T.; Sano, H.; Yamada, N. *Chem. Lett.* **1987**, 405−408.
(5) Chandler, B. D.; Kendell, S.; Doan, H.; Korkosz, R.; Grabow, L. C.; Pursell, C. J. *ACS Catal.* **2012**, *2*, 684−694.
(6) Arrii, S.; Morfin, F.; Renouprez, A. J.; Rousset, J. L. *J. Am. Chem. Soc.* **2004**, *126*, 1199−1205.
(7) Haruta, M.; Tsubota, S.; Kobayashi, T.; Kageyama, H.; Genet, M. J.; Delmon, B. *J. Catal.* **1993**, *144*, 175−192.
(8) Lin, H. Y.; Chen, Y. W. *Ind. Eng. Chem. Res.* **2005**, *44*, 4569−4576.
(9) Sa, J.; Taylor, S. F. R.; Daly, H.; Goguet, A.; Tiruvalam, R.; He, Q.; Kiely, C. J.; Hutchings, G. J.; Hardacre, C. *ACS Catal.* **2012**, *2*, 552−560.
(10) Zhang, G. R.; Zhao, D.; Feng, Y. Y.; Zhang, B. S.; Su, D. S.; Liu, G.; Xu, B. Q. *ACS Nano* **2012**, *6*, 2226−2236.
(11) He, D. P.; Jiao, X. D.; Jiang, P.; Wang, J.; Xu, B. Q. *Green Chem.* **2012**, *14*, 111−116.
(12) Sun, K. Q.; Hong, Y. C.; Zhang, G. R.; Xu, B. Q. *ACS Catal.* **2011**, *1*, 1336−1346.
(13) Zhang, X.; Shi, H.; Xu, B. Q. *J. Catal.* **2011**, *279*, 75−87.
(14) Haruta, M. *Catal. Today* **1997**, *36*, 153−166.
(15) Haruta, M. *Gold Bull.* **2004**, *37*, 27−36.
(16) Tsubota, S.; Cunningham, D. A. H.; Bando, Y.; Haruta, M. *Stud. Surf. Sci. Catal.* **1995**, *91*, 227−235.
(17) Cunningham, D. A. H.; Vogel, W.; Kageyama, H.; Tsubota, S.; Haruta, M. *J. Catal.* **1998**, *177*, 1−10.
(18) Wolf, A.; Schüth, F. *Appl. Catal., A* **2002**, *226*, 1−13.
(19) Li, L.; Wang, A. Q.; Qiao, B.; Lin, J.; Huang, Y. Q.; Wang, X. D.; Zhang, T. *J. Catal.* **2013**, *299*, 90−100.
(20) Costello, C. K.; Yang, J. H.; Law, H. Y.; Wang, Y.; Lin, J. N.; Marks, L. D.; Kung, M. C.; Kung, H. H. *Appl. Catal., A* **2003**, *243*, 15−24.
(21) Akita, T.; Lu, P.; Ichikawa, S.; Tanaka, K.; Haruta, M. *Surf. Interface Anal.* **2001**, *31*, 73−78.
(22) Daté, M.; Ichihashi, Y.; Yamashita, T.; Chiorino, A.; Boccuzzi, F.; Haruta, M. *Catal. Today* **2002**, *72*, 89−94.
(23) Schumacher, B.; Plzak, V.; Kinne, M.; Behm, R. J. *Catal. Lett.* **2003**, *89*, 109−114.
(24) Zanella, R.; Louis, C. *Catal. Today* **2005**, *107*−*108*, 768−777.
(25) Vogel, W.; Cunningham, D. A. H.; Tanaka, K.; Haruta, M. *Catal. Lett.* **1996**, *40*, 175−181.
(26) Schubert, M. M.; Plzak, V.; Garche, J.; Behm, R. J. *Catal. Lett.* **2001**, *76*, 143−150.
(27) Konova, P.; Naydenov, A.; Venkov, C.; Mehandjiev, D.; Andreeva, D.; Tabakova, T. *J. Mol. Catal. A: Chem.* **2004**, *213*, 235−240.
(28) Moreau, F.; Bond, G. C. *Appl. Catal., A* **2006**, *302*, 110−117.
(29) Zanella, R.; Rodríguez-González, V.; Arzola, Y.; Moreno-Rodriguez, A. *ACS Catal.* **2012**, *2*, 1−11.
(30) Yan, W. F.; Mahurin, S. M.; Pan, Z. W.; Overbury, S. H.; Dai, S. *J. Am. Chem. Soc.* **2005**, *127*, 10480−10481.
(31) Zhu, H. G.; Ma, Z.; Overbury, S. H.; Dai, S. *Catal. Lett.* **2007**, *116*, 128−135.
(32) Jin, R. C. *Nanotechnol. Rev.* **2012**, *1*, 31−56.
(33) Piao, Y.; Kim, J.; Bin Na, H.; Kim, D.; Baek, J. S.; Ko, M. K.; Lee, J. H.; Shokouhimehr, M.; Hyeon, T. *Nat. Mater.* **2008**, *7*, 242−247.
(34) Sui, Y. M.; Fu, W. Y.; Zeng, Y.; Yang, H. B.; Zhang, Y. Y.; Chen, H.; Li, Y. X.; Li, M. H.; Zou, G. T. *Angew. Chem., Int. Ed.* **2010**, *49*, 4282−4285.
(35) An, K.; Kwon, S. G.; Park, M.; Bin Na, H.; Baik, S. I.; Yu, J. H.; Kim, D.; Son, J. S.; Kim, Y. W.; Song, I. C.; Moon, W. K.; Park, H. M.; Hyeon, T. *Nano Lett.* **2008**, *8*, 4252−4258.
(36) Fei, J. B.; Cui, Y.; Yan, X. H.; Qi, W.; Yang, Y.; Wang, K. W.; He, Q.; Li, J. B. *Adv. Mater.* **2008**, *20*, 452−456.
(37) Wang, L. Z.; Tang, F. Q.; Ozawa, K.; Chen, Z. G.; Mukherj, A.; Zhu, Y. C.; Zou, J.; Cheng, H. M.; Lu, G. Q. *Angew. Chem., Int. Ed.* **2009**, *48*, 7048−7051.
(38) Sun, X. M.; Liu, J. F.; Li, Y. D. *Chem.—Eur. J.* **2006**, *12*, 2039−2047.
(39) Fei, Z. Y.; He, S. C.; Li, L.; Ji, W. J.; Au, C. T. *Chem. Commun.* **2012**, *48*, 853−855.
(40) Hermanek, M.; Zboril, R.; Medrik, N.; Pechousek, J.; Gregor, C. *J. Am. Chem. Soc.* **2007**, *129*, 10929−10936.
(41) Liu, X. H.; Zhang, J.; Guo, X. Z.; Wu, S. H.; Wang, S. R. *Nanotechnology* **2010**, *21*, No. 095501.
(42) Wu, C. Z.; Yin, P.; Zhu, X.; OuYang, C. Z.; Xie, Y. *J. Phys. Chem. B* **2006**, *110*, 17806−17812.
(43) Kung, H. H.; Kung, M. C.; Costello, C. K. *J. Catal.* **2003**, *216*, 425−432.
(44) Pattrick, G.; van der Lingen, E.; Corti, C. W.; Holliday, R. J.; Thompson, D. T. *Top. Catal.* **2004**, *30*−*31*, 273−279.
(45) Bond, G. C.; Thompson, D. T. *Gold Bull.* **2000**, *33*, 41−51.
(46) Haruta, M. *CATTECH* **2002**, *6*, 102−115.
(47) Carabineiro, S. A. C.; Bogdanchikova, N.; Tavares, P. B.; Figueiredo, J. *RSC Adv.* **2012**, *2*, 2957−2965.
(48) Zhou, H. P.; Wu, H. S.; Shen, J.; Yin, A. X.; Sun, L. D.; Yan, C. H. *J. Am. Chem. Soc.* **2010**, *132*, 4998−4999.
(49) Boccuzzi, F.; Chiorino, A.; Manzoli, M.; Lu, P.; Akita, T.; Ichikawa, S.; Haruta, M. *J. Catal.* **2001**, *202*, 256−267.
(50) Nie, X. T.; Qian, H. F.; Ge, Q. J.; Xu, H. Y.; Jin, R. C. *ACS Nano* **2012**, *6*, 6014−6022.
(51) Gaur, S.; Miller, J. T.; Stellwagen, D.; Sanampudi, A.; Kumard, C. S. S. R.; Spivey, J. J. *Phys. Chem. Chem. Phys.* **2012**, *14*, 1627−1634.
(52) Widmann, D.; Leppelt, R.; Behm, R. J. *J. Catal.* **2007**, *251*, 437−442.
(53) Li, L.; Wang, A.; Qiao, B.; Lin, J.; Huang, Y.; Wang, X.; Zhang, T. *J. Catal.* **2013**, *299*, 90−100.
(54) Fei, Z. Y.; Sun, B.; Zhao, L.; Ji, W. J.; Au, C. T. *Chem.—Eur. J.* **2013**, *19*, 6480−6487.
(55) Santos, V. P.; Pereira, M. F. R.; Órfão, J. J. M.; Figueiredo, J. L. *Appl. Catal., B* **2010**, *99*, 353−363.
(56) Solsona, B.; Davies, T. E.; Garcia, T.; Vázquez, I.; Dejoz, A.; Taylor, S. H. *Appl. Catal.. B* **2008**, *84*, 176−184.
(57) Hodnett, B.K. In *Heterogeneous Catalytic Oxidation*; Wiley: West Sussex, U.K., 2000; pp. 86−90.
(58) Xu, X. J.; Fu, Q.; Guo, X. G.; Bao, X. H. *ACS Catal.* **2013**, *3*, 1810−1818.
(59) Xue, L.; Zhang, C. B.; He, H.; Teraoka, Y. *Appl. Catal., B* **2007**, *75*, 167−174.
(60) Wu, Y.; Zhang, J.; Xiao, L.; Chen, F. *Appl. Catal., B* **2009**, *88*, 525−532.
(61) Cao, J. L.; Wang, Y.; Yu, X. L.; Wang, S. R.; Wu, S. H.; Yuan, Z. Y. *Appl. Catal., B* **2008**, *79*, 26−34.
(62) Dupin, J. C.; Gonbeau, D.; Vinatier, P.; Levasseur, A. *Phys. Chem. Chem. Phys.* **2000**, *2*, 1319−1324.
(63) Venugopal, A.; Scurrell, M. S. *Appl. Catal., A* **2004**, *258*, 241−249.
(64) Daniells, S. T.; Overweg, A. R.; Makkee, M.; Moulijn, J. A. *J. Catal.* **2005**, *230*, 52−65.